Supplementary Materials

Supplementary Figure 1: Sequence, structure and expression of the CD3. NK-92 and T cell activation pathways.

Supplementary Figure 2: kinetic properties of transduced TCR in TCR-NK-92 cells and major kinases phosphorylation

Supplementary Figure 3: Expression of major lymphocyte markers as determined by flow cytometry and CyTOF.

Supplementary Figure 4: Glycolysis profile of TCR-NK-92 cells

Supplementary Figure 5: Characterization of TCR-NK-92 adhesion zone organization.

Supplementary Data (movie): Annexin V live assay. Movie S1, S2 and S3

Supplementary Figure 1

a

MKWKALFTAAILQAQLPITEAQSFGLLDPKLCYLLDGILFIYGVILTALFLRVKFSRSAD

APAYQQGQNQLYNELNLGRREEYDVLDKRRGRDPEMGGKPQRRKNPQEGLYNELQKDKMA

EAYSEIGMKGERRRGKGHDGLYQGLSTATKDTYDALHMQALPPRVKQTLNFDLLKLAGDV

ESNPGPMQSGTHWRVLGLCLLSVGVWGQDGNEEMGGITQTPYKVSISGTTVILTCPQYPGSEIL
WQHNDKNIGGDEDDKNIGSDEDHLSLKEFSELEQSGYYVCYPRGSKPEDANFYLYLRARVCE

NCMEMDVMSVATIVIVDICITGGLLLLVYYWSKNRKAKAKPVTRGAGAGGRQRGQNKERP

PPVPNPDYEPIRKGQRDLYSGLNQRRIEGRGSLLTCGDVEENPGPMEHSTFLSGLVLATLLSQVS
PFKIPIEELEDRVFVNCNTSITWVEGTVGTLLSDITRLDLGKRILDPRGIYRCNGTDIYKDKESTV
QVHYRMCQSCVELDPATVAGIIVTDVIATLLLALGVFCFAGHETGRLSGAADTQALLRNDQVY
QPLRDRDDAQYSHLGGNWARNKQCTNYALLKLAGDVESNPGPMEQGKGLAVLILAIILLQGT
LAQSIKGNHLVKVYDYQEDGSVLLTCDAEAKNITWFKDGKMIGFLTEDKKKWNLGSNAKDPR
GMYQCKGSQNKSKPLQVYYRMCQNCIELNAATISGFLFAEIVSIFVLAVGVYFIAGQDGVRQSR
ASDKQTLLPNDQLYQPLKDREDDQYSHLQGNQLRRN

b

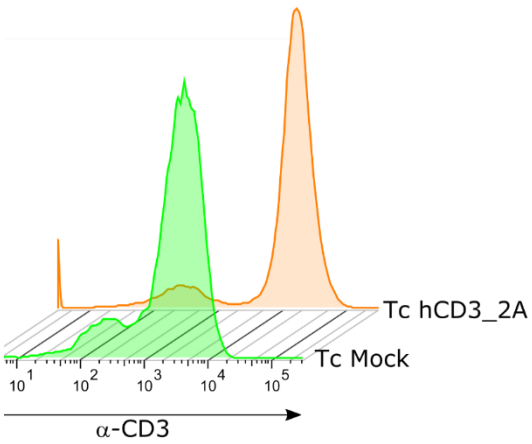

c

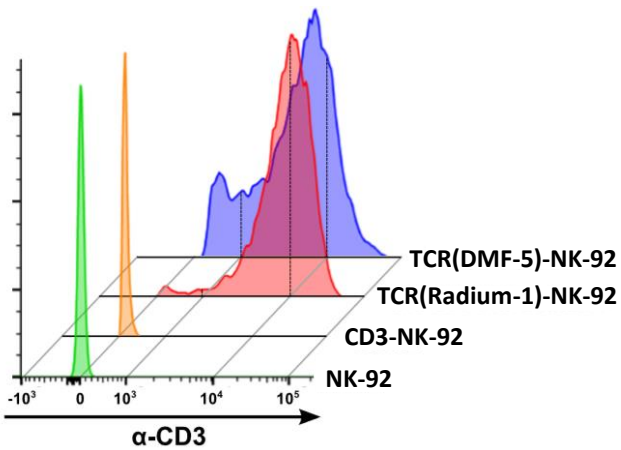

d

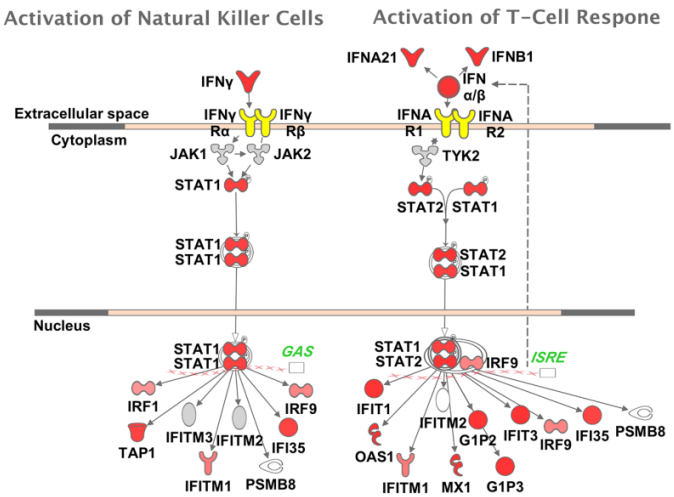

Figure S1: **a**) Design of the human CD3 construct with the sequences of the different CD3 units, in blue the different 2A sequences are shown and used in the following order: F2A, T2A and E2A, respectively. **b**) Representative experiment showing the expression of hCD3_2A construct in T cells and detected by flow cytometry. **c)** Representative experiment showing CD3 expression in NK-92, CD3-NK-92, TCR(Radium-1)-NK-92 and TCR(DMF-5)-NK-92. **d)** Activated pathways in TCR-NK-92 cells as determined by IPA® (Qiagen) based on differentially expressed genes in TCR-NK-92 cells compared to NK-92 and CD3-NK-92 cells (RNA-seq data).

Supplementary Figure 2

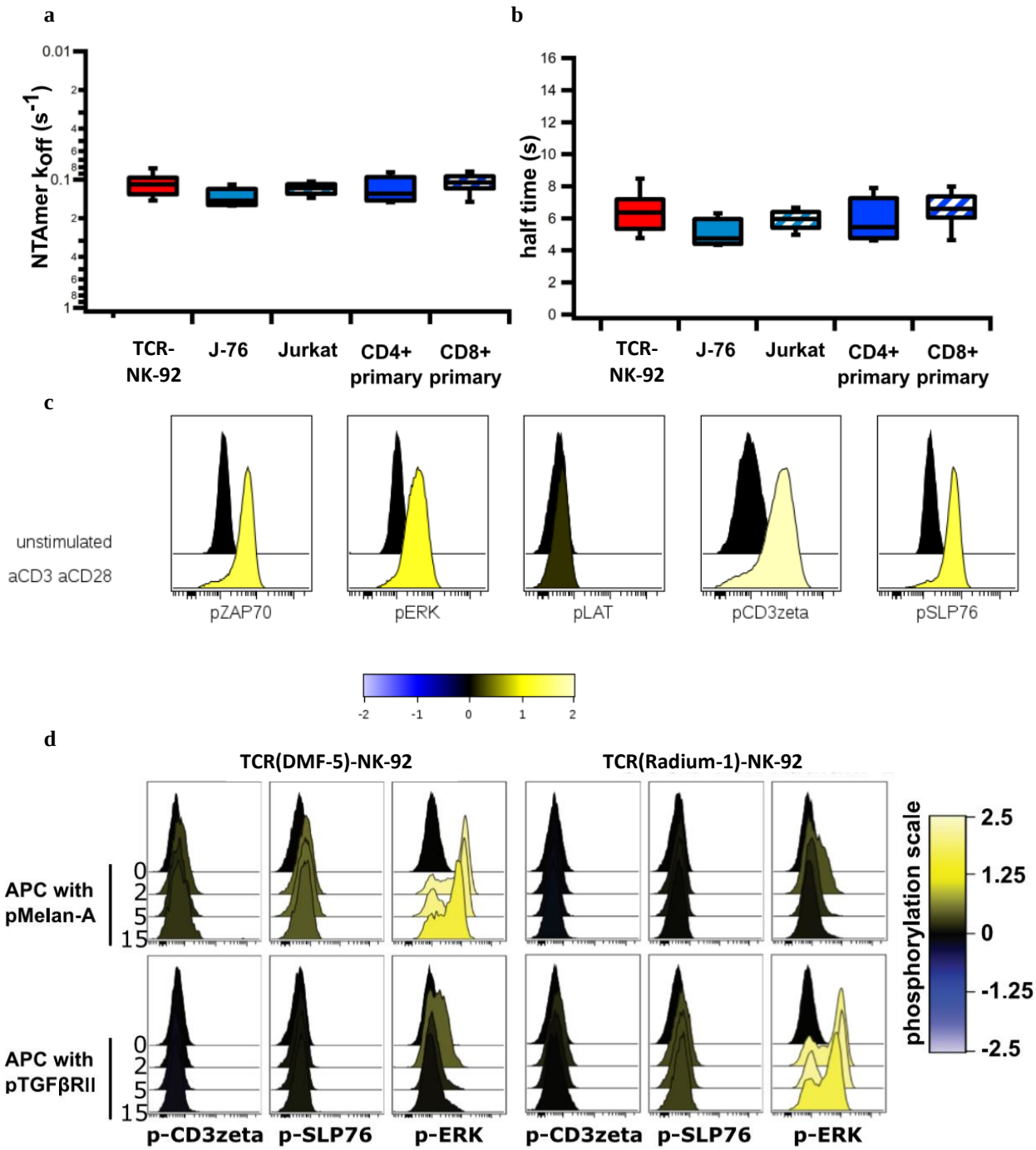

Figure S2: **a**)-**b**) Comparison of structural avidity between CD3-NK-92 and a panel of T cells expressing the Melan-A-specific DMF-5 TCR. Scatter plots represent direct comparison of TCR-ligand monomeric dissociation kinetics (koff(s-1) and half-lives (s)) using the 2-color NTAmer technology. Values were obtained in parallel experiments performed on pure populations of DMF-5 TCR-transduced Jurkat, J76, CD3-NK-92 and primary CD4+ or CD8+ T cells. (n=4 to 7 independent experiments for each cell type). Error bars represents SD. **c)** Stimulation of CD3-NK-92 with CD3/CD28 antibodies was performed as follows: the cells were incubated with biotinylated anti-CD3/CD28 antibodies, cross-linked for 2min with avidin. Specific TCR signaling was detected by phospho-specific flow cytometry. Histograms show induced phosphorylation levels of selected known proteins in unstimulated and stimulated TCR-NK-92. Representative experiment of two separated ones. **d)** Phosphorylation of TCR signaling proteins (CD3zeta, SLP76, ERK, ZAP70) in TCR-NK-92 (either DMF-5 TCR or Radium-1 TCR) upon stimulation with APCs loaded with either relevant peptide (pMelan-A or pTGFβRII, respectively) or irrelevant peptide detected by phospho-specific flow cytometry. Histogram overlays from one representative experiment (n=4). TCR-induced phosphorylation was measured at 2, 5, 15 min. The color code shows induced phosphorylation level relative to unstimulated cells using the inverse hyperbolic sine (arcsinh) transformation of the median fluorescence intensity.

Supplementary Figure 3

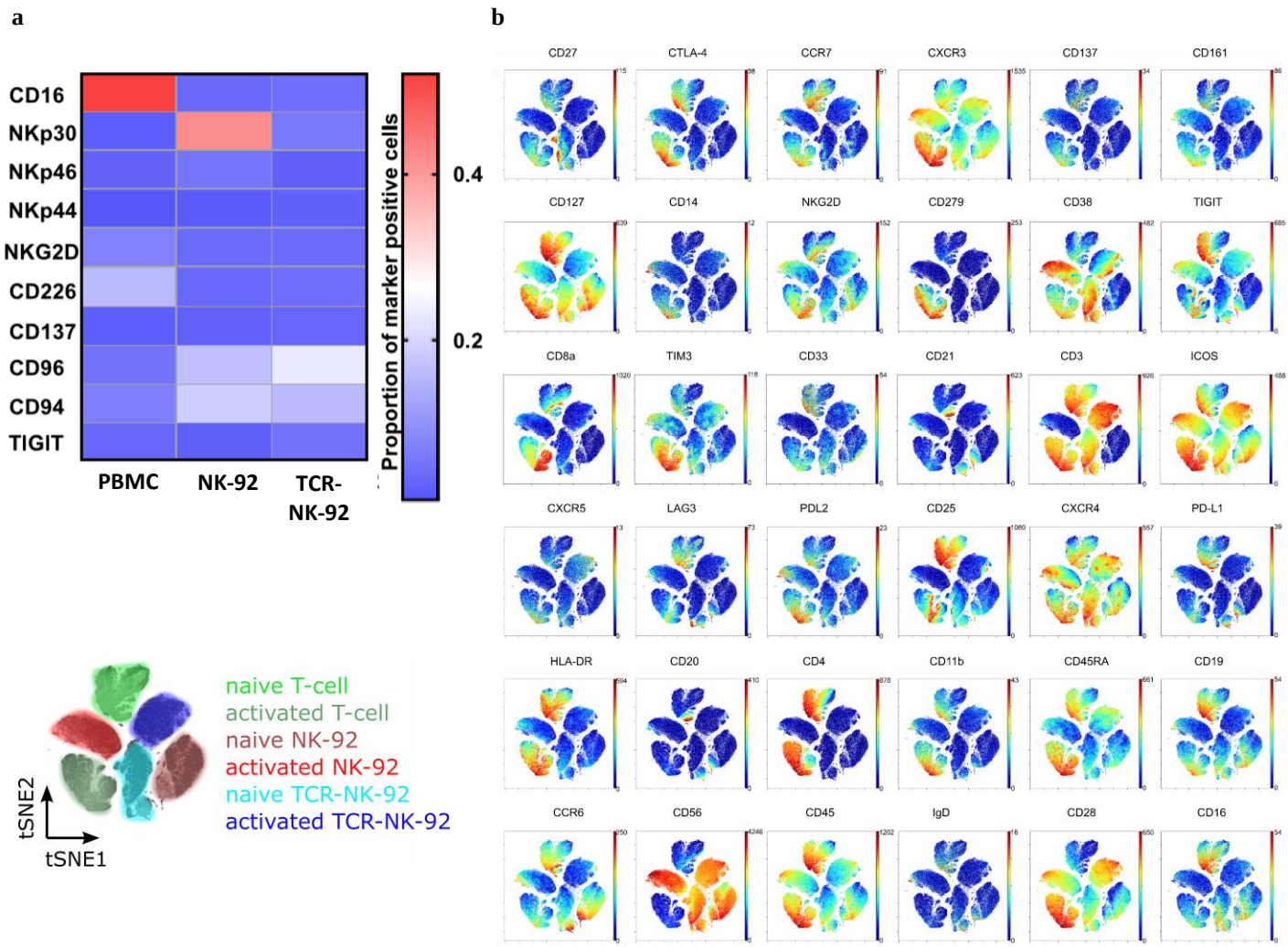

Figure S3: **a**) Heat map analysis of activating and inhibitory receptor phenotype in PBMC, NK-92 and TCR-NK-92. Blue-to-red transition represents the mean fluorescence intensity (MFI) of the surface expression of different activating and inhibitory receptors. **b)** Complete outcome of ViSNE analysis on TCR-NK-92, NK-92 and T cells before and after activation.

Supplementary Figure 4

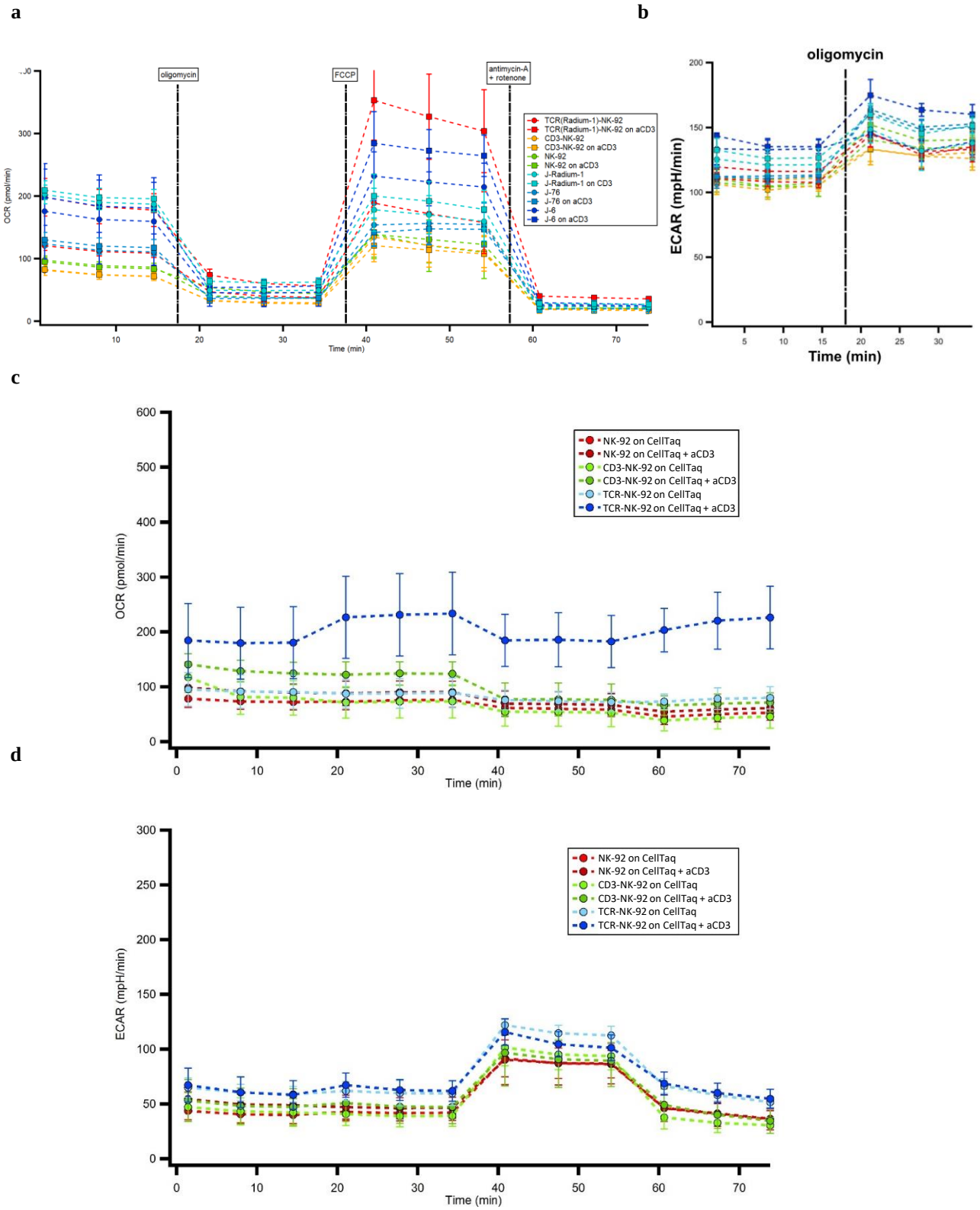

Figure S4: **a**) Oxygen Consumption Rate (OCR) of NK-92, CD3-NK-92, TCR(Radium-1)-NK-92, J6, J76 and J Radium-1 overtime, in the presence or not of anti-CD3 (aCD3). Mitochondrial respiration function (expressed as OCR rate) was measured, first at baseline and, then, probed by the serial addition of oligomycin, FCCP and antimycin-A/rotenone (anti-A + rot) as indicated in the graph. (n= 21). Error bars represent SD. **b)** ExtraCellular Acidification Rate (ECAR) of NK-92, CD3-NK-92, TCR-NK-92, J6, J76 and J Radium-1, either CD3 treated or untreated, before and after addition of oligomycin is shown. **c)-d)** OCR and ECAR of NK-92, CD3-NK-92 and TCR-NK-92 on CD3 coated surface in the context of a glycostress experiment (n=21). Error bars represent SD.

Supplementary Figure 5

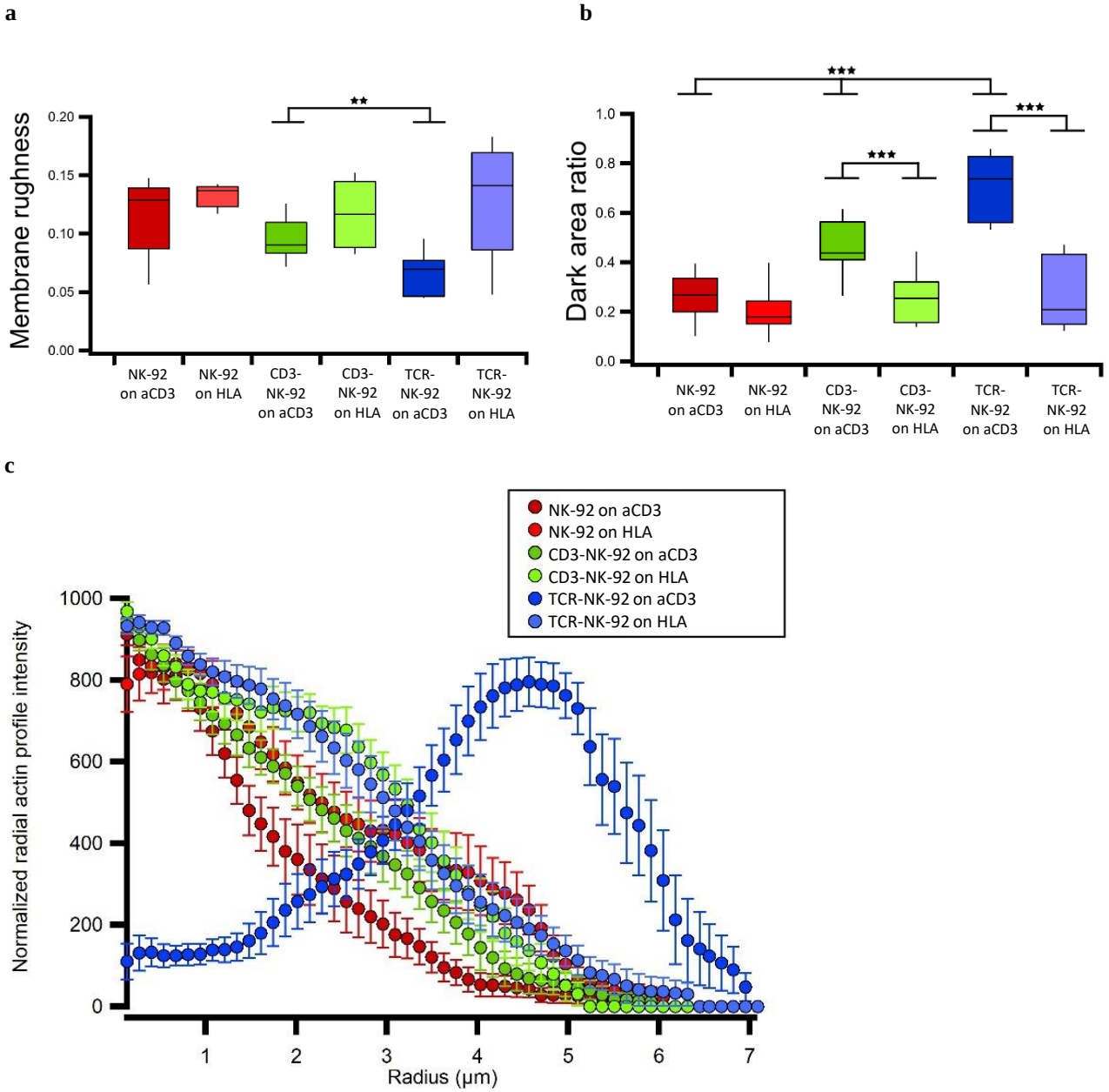

Figure S5: **a**) TCR-NK-92 exhibits flat membrane at the contact surface zone**.** Membrane roughness was assessed as described in Dillard et al.[27] n= at least 50 for each condition. **b)** TCR-NK-92 exhibits large tight adhesion surface at the contact surface zone. Dark area membrane in RICM was assessed as described in Dillard et al. [27] n= at least 50 for each condition. **c)** TCR-NK-92 exhibits ring actin organization. Normalized radial actin organization was assessed on TIRF images as described in Dillard et al [27]